Effect of molybdenum on the behaviour of caesium in uranium dioxide at high temperature

C. Panetier, L. Sarrasin, C. Gaillard, Y. Pipon, T. Wiss, A. Benedetti, O. Dieste, D. Mangin, R. Ducher, R. Dubourg, et al.

Effect of molybdenum on the behaviour of caesium in uranium dioxide at high temperature

C. Panetier[a], L. Sarrasin[a], C. Gaillard[a]*, Y. Pipon[a,b], T. Wiss[c], A. Benedetti[c], O. Dieste[c], D. Mangin[d], R. Ducher[e], R. Dubourg[e], N. Moncoffre[a]

[a] Univ Lyon, Univ Claude Bernard Lyon 1, CNRS/IN2P3, IP2I Lyon, UMR 5822, F-69622, Villeurbanne, France

[b] Univ Lyon, UCBL, IUT Lyon-1, Département chimie, F-69622, Lyon, France

[c] European Commission, DG Joint Research Centre, Directorate G – Nuclear Safety & Security, PO box 2340, D-76125 Karlsruhe, Germany

[d] IJL, Université de Lorraine, CNRS : UMR7198 – CS 14234 54042 Nancy Cedex, France

[e] IRSN, LETR – BP3 13115 St-Paul-Lez-Durance Cedex, France

* corresponding author gaillard@ipnl.in2p3.fr, IP2I Lyon, 4 rue Enrico Fermi, 69622 Villeurbanne cedex, France

Keywords

Caesium, molybdenum, UO_2, bubble-precipitate pairs, thermal annealing

Highlights

- The effect of a metallic fission product on Cs behaviour and its release in UO_2 was investigated as a relevant aspect of fuel safety
- Mo and Cs were co-implanted in UO_2
- Mo metallic precipitates anchor Cs bubbles and hinder their migration
- The role of dislocations on the nucleation of bubbles and metallic precipitates is highlighted

Abstract

This study aims to evaluate the influence of a metallic fission product, molybdenum, on the behaviour of caesium in UO_2 at high temperature (1600°C) under reducing atmosphere. Both elements were successively introduced by ion implantation (firstly Mo, then Cs) at room temperature at a fluence of 10^{16} ions/cm². We show that in these co-implanted samples, the defects created by the Mo implantation render possible the nucleation of nanometric size bubbles during Cs implantation at room temperature. SIMS and TEM techniques were coupled in order to characterize the migration of both elements, as well as the UO_2 microstructure evolution after annealing at 1600°C. We found that Mo is more mobile in presence of Cs, which may be related to an increase of available vacancies in the material produced by Cs implantation. On the contrary, the concentration profiles of Cs remain quite similar than when it is solely implanted, and its release percentage remain the same both in absence and presence of Mo. After annealing, both elements are found to be associated as Mo metallic precipitates and Cs bubbles distributed over the same depth (~150 nm). Comparing with the Cs bubbles distribution in absence of Mo, it is clear that the formation of Mo metallic precipitates hinders the Cs bubble migration. Our study highlights the role of dislocations on the nucleation of bubbles and metallic precipitates.

1. Introduction

The experience feedback from the accident of Fukushima Dai-Ichi (Japan) in March 2011 has strengthened the importance of developing predictive capabilities about the evolution of accidental sequences in nuclear facilities. Particularly interesting are the amount, chemical speciation and isotope inventory of radionuclides produced by fission, which could be released to the environment. Indeed, in the case of an accident in a Pressurized Water Reactor (PWR), temperature and irradiation increase may cause the rupture of the fuel's cladding and expose the nuclear fuel to oxidizing conditions. Consequently, the Fission Products (FPs) may escape from the fuel and possibly be released into the environment.

In view to elaborate a reliable modelling of the phenomena occurring during accidental conditions, it is crucial to understand precisely the behaviour of each fission product in the fuel. Caesium is a volatile FP produced with a high yield (~6% for ^{137}Cs). The ^{137}Cs isotope (T = 30.7 years) is very radiotoxic, and highly susceptible to be released at high temperature. Under normal operating conditions, most of Cs remains in the UO_2 matrix [1] and may accumulate at the pellet periphery or in the HBS zone [2, 3]. Different accidental conditions were reproduced during semi-integral research programs like VERCORS, VERDON and VEGA [4-7]. These tests consisted in submitting irradiated nuclear fuel to high temperature (>2000°C) under different atmospheres and measuring the nature and quantity of released FPs. The results from these programs showed that under reducing conditions the amount of released Cs mainly depends on the temperature reached in the fuel, this release being total above 2350°C. However, the other experimental conditions (atmosphere, burn-up) also affect the Cs release: for example, an increase of burn-up enhances the release kinetics of Cs.

In normal operating conditions, the nuclear spent fuel also contains FPs that form metallic precipitates, known as white inclusions [8]. They are composed of Mo, Tc and noble metals like Ru, Rh and Pd. The composition of these white phases depends on the fuel burn-up, UO_2 stoichiometry and temperature. For instance, the size of inclusions diminishes when decreasing Mo concentrations [9-11]. Transmission Electron Microscopy (TEM) characterizations of irradiated fuel evidenced that these inclusions may be associated with gas bubbles in the case of high burn-up values or following a high temperature annealing, i.e. experimental conditions that could be compared to accidental operating conditions. In 1966, Whapham observed an association of gas bubbles with metallic precipitates after a one hour annealing at 1500°C of UO_2 pellet previously irradiated with a neutron flux [12]. Thomas et al. [1] in LWR fuel, Manley [13], and Hastings in a PWR fuel [14] obtained practically the same results, both in highly irradiated fuel and at high operating temperature (up to 1700°C). The latter author measured bubbles with a diameter ranging between 100 and 400 nm, associated with 20 nm precipitates. The same observation has been made by Walker et al. [15], who analysed a transient tested BWR fuel by TEM. They measured the evolution of gas bubbles and precipitates size as a function of the radial position r/r_0 and temperature. Between r/r_0 = 0.66 and 0.46, which corresponds to estimated temperatures of 1125°C and 1550 °C respectively, the bubble radius increases from 83 nm to 350 nm while the precipitates radius increases from 50 to 100 nm. This growth goes with a decrease of the number of bubbles and precipitates. Ray et al. [16], who analysed a LWR irradiated fuel (burn-up 4.5%) by TEM, also noticed the presence of a uniform population of very small fission gas bubbles across the whole fuel cross section, with an average diameter of about 8 nm, linked to precipitates with about the same size distribution. This population is shown to disappear after submitting this fuel to a further power increases up to a maximum of 420 W/cm, which leads to a temperature increase of 300°C at the centre of the pellet. However, a population of large fission gas bubbles (30-50 nm diameter) attached to large metallic precipitates was present on the dislocation networks.

Many of these authors suggest that the metallic precipitates would act as nucleation sites for fission gas bubbles and that the bubble-precipitate association would retard the rate of bubble coalescence and restrain the migration of bubbles in UO_2. Walker *et al.* also noted an influence of the local mechanical restraint pressure on the evolution of precipitate-bubble pairs [15]. Compressive stress may hinder the pair growth and the subsequent bubble interlinkage.

All these studies show that the release of volatile FPs from UO_2 fuel in accidental conditions may result from complex mechanisms. We have carried out an extensive study of the Cs migration in UO_2 at high temperature, by decorrelating different conditions that may influence the Cs behaviour (temperature, irradiation, presence of other FPs). As a first step, we have characterized its thermal behaviour under reducing atmosphere when no other FPs are present. Cs was introduced at a 10^{15} at/cm² fluence in UO_2 pellets by ion implantation (800 keV) in order to simulate its formation by fission in the fuel. After high temperature annealing (1000 to 1600°C), the Cs migration was characterized by coupling SIMS (Secondary Ion Mass Spectrometry) and TEM analysis. We observed the formation of nanometric spherical Cs bubbles after annealing at 1000°C. This phenomenon is in agreement with a previous work led at low temperature (600°C) [17]. At higher temperature, a strong release of Cs was measured (~60 % after a 12 h annealing at 1600 °C), while the remaining caesium near the surface consisted of spherical bubbles and large faceted bubbles probably formed as the result of an Ostwald ripening growth [18].

In the present work, we have used the same methodology to assess the effect of an abundant, metallic (under reducing annealing conditions) fission product, Mo, on the behaviour of caesium at high temperature (1600°C). Mo and Cs were successively implanted in UO_2 pellets before annealing. Then, SIMS was used to follow the evolution of Mo and Cs concentration profiles and the UO_2 microstructural changes were characterised by TEM.

2. Experimental

2.1. Materials

Depleted UO_2 disks (0.2 at. % of ^{235}U) supplied by FRAMATOME (ex-AREVA NP) were sintered at 1750 °C under a reducing atmosphere (Ar/H_2-5%) during 5 h, in order to obtain a high bulk density value (97.5 % of the theoretical density). Each pellet is a cylinder with a height of (1.7 ± 0.2) mm and diameter of (8.6 ± 0.4) mm. The mean grain size distribution is centred at 11 µm.

The pellets were polished on one side by the PRIMEVerre company (Montpellier, France). Their mean surface roughness is of 5 nm, as measured by optical interferometry on a FOGALE NANOTECH device (LaMCoS laboratory, INSA Lyon, France). After polishing, the samples were annealed at 1000 °C during 10 h in a PEKLY© tubular furnace under vacuum (10^{-7} mbar), in order to degas particles adsorbed on the surface. Then, the samples were annealed at 1600 °C for 4 h in a NABERTHERM© tubular furnace under a 5 % H_2/Ar gas mixture in order to anneal the polishing damage, as verified by Doppler Broadening Positron Annihilation Spectroscopy (PAS-DBS) [19], while maintaining the $UO_{2.00}$ stoichiometry.

2.2. Ion implantation

Caesium and molybdenum ions were introduced in the pellets by ion implantation. The samples were implanted first with 400 keV $^{95}Mo^{+}$ ions and then with 800 keV $^{133}Cs^{2+}$ ions at IP2I (Institut de Physique des deux Infinis) Lyon, France, using the IMIO400 accelerator facility. A cooling device was used to maintain the sample temperature at 15 °C (samples were fixed on the sample holder using

carbon tape) and under vacuum (< 5 × 10^{-6} mbar) to prevent any oxidation. We chose an implantation fluence of 10^{16} at cm^{-2} for both elements, which was achieved using an average dose rate of 3 10^{11} at/cm²/s.

Simulations of Cs and Mo implantation were performed using the SRIM 2013 software [20] in the full cascade mode. We considered a density of 10.7 g cm^{-3} and displacement energies were set to 40 eV and 20 eV for uranium atoms and oxygen atoms, respectively, as determined by Soullard *et al* [21]. The resulting Cs and Mo depth profiles, shown in Figure 1, are quasi-Gaussian distributions whose characteristics are given in Table 1. The choice of these implantation conditions allows one to obtain an overlap between the Mo and Cs concentration profiles, which would favour any interactions between these two elements during annealing (see Figure 1). The damage distribution peak (measured in dpa, displacements per atom) is centred at 80 nm for Cs and 50 nm for Mo.

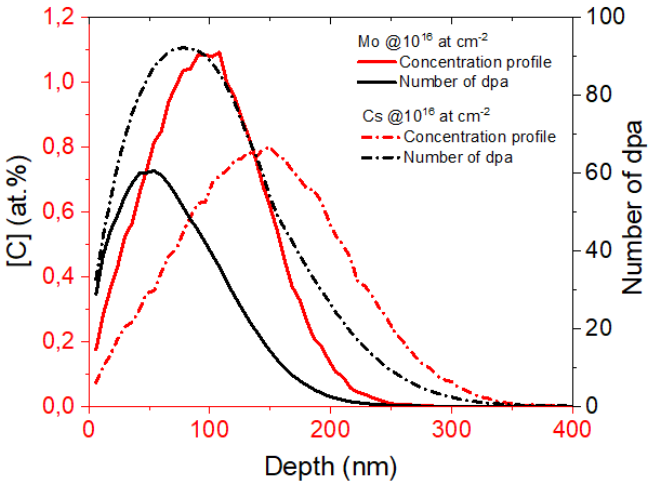

Figure 1: Cs and Mo concentration and dpa (displacements per atom) profiles in UO_2 after implantation at an energy of 800 and 400 keV, respectively, and at a fluence of 10^{16} at/cm² (SRIM calculations).

Table 1 : Characteristics of the concentration and dpa (displacement per atom) profiles of Cs and Mo after implantation in UO_2, as calculated by SRIM. Rp is the projected range of the implanted ions and Rd is the mean range of damages created by implantation.

		Concentration profile		dpa profile	
	Implantation Energy (keV)	Rp (nm)	at.% at Rp	Rd (nm)	dpa at Rd
Mo	400	95	1	50	60
Cs	800	140	0.8	80	90

2.3. Sample thermal treatments and characterization

After implantation, the as-implanted samples were annealed at 1600 °C for 4 hours in the NABERTHERM© furnace under reducing atmosphere (5% H_2/Ar).

The caesium and molybdenum concentration profiles were measured before and after annealing by SIMS. Analyses were performed on a CAMECA IMS 7f spectrometer at the Jean Lamour Institute (IJL), Nancy, France. This instrument is equipped with an eucentric rotating sample stage (see [22] for more details), to improve the depth resolution by inhibiting the surface roughening during SIMS analysis of poly-crystalline materials. We have previously shown that this device allows one to minimize the preferential grain abrasion of UO_2 polycrystalline pellets, therefore yielding reproducible concentration profiles [18, 23, 24]. A primary beam of 10 keV O_2^+ ions with a current of 140 nA was used. The raster size was 250 × 250 µm^2 on the UO_2 sample surfaces and the velocity of the eucentric stage was set to 8 rpm. Secondary ions ($^{238}U^{16}O^+$, $^{133}Cs^+$, $^{95}Mo^+$) were collected on the raster central part (62 µm in diameter). The conversion of chronograms into depth profiles was made according to the procedure described in [18, 24]. At least three craters were made on each sample, and consequently three depth profiles were obtained which were averaged.

Microstructural changes in the UO_2 samples were characterised by TEM analysis, performed at the JRC (Joint Research Centre) Karlsruhe, Germany. A FEI™ VERSA 3D Focused Ion Beam (FIB), was used to prepare electron transparent lamellae from the UO_2 samples. Samples were first covered with a sputtered 100-200 nm gold layer and then a double platinum layer was deposited in the FIB, using the electron beam first and the ion beam then, to protect the surface during milling operations. Once the Pt deposit was made, two trenches were cut with the Ga^+ ion beam, then the remaining lamella was cut free from the sample, removed with an Omniprobe needle and attached to a Cu grid. Thinning and final cleaning of the lamella were then performed at decreasing voltages, taking extreme care not to consume the protecting layer and to avoid introducing artefacts in the sample. The thickness of each lamella is around 50-70 nm, as determined by EELS by calculating the ratio between the zero loss peak (ZLP) and the total counts, accounting for the total inelastic mean free path (65 +/- 15 nm; see supplementary information for details) and the sample composition. The lamellae were analysed by a FEI™ Tecnai G2 TEM used at 120 kV [25]. Bright field images and Selective Area Diffraction Patterns (SAED) were recorded on several areas, as well as Energy Dispersive X-ray spectra. The use of a nanoprobe was not possible so that single particles could not be analysed neither by EELS nor by EDX.

As a summary, Table 2 presents the composition, thermal treatments and analysis performed in UO_2 samples presented in this paper.

Table 2 : Summary of UO_2 samples preparation and analysis presented in this paper.

Implanted elements	Fluence (at/cm²)	Thermal treatment		Analysis	
		T°C	Time (h)	SIMS	TEM
Mo	10^{16}	none		x	
		1600	4	x	
Cs	10^{16}	none		x	
		1600	4	x	
Mo + Cs	10^{16} + 10^{16}	none		x	x
		1600	4	x	x

3. Results

3.1. Evolution of Mo and Cs concentration profiles under thermal treatments

Figure (a) displays the molybdenum and caesium profiles in UO_2 obtained by SIMS before and after annealing at 1600°C for 4 hours. The as-implanted molybdenum profile is centred at 85 nm with a maximum concentration of 1 at.%, while the as-implanted Cs profile is centred at 140 nm with a maximum concentration of 0.6 at.%. The latter concentration is slightly below that expected from SRIM calculations (0.8 at.%), but we observe that the Cs as-implanted profile is also more spread out in depth. It can be attributed to the effect of the pre-implantation of Mo and the defects created in the materials.

We observe that annealing at 1600°C entails a migration of both elements towards the surface. No release of molybdenum is observed and its migration results in an increase of its maximum concentration to 1.4 at.% at a 50 nm depth. At the same time, a strong release of Cs is measured (57±5 %). This release was measured from the SIMS profile area before and after annealing. The remaining Cs atoms are distributed in the first 200 nm of the sample. In order to highlight the effect of the co-implantation on the behaviour of each element, Figure 2 b) c) shows a comparison of the Mo and Cs concentration profiles after annealing at 1600°C, both in presence of only one element and in case they are co-implanted. Alone, molybdenum is not mobile in UO_2 after this annealing (Figure 2 (b)). On the contrary, the final Cs concentration profiles are quite similar after annealing (Figure 2 (c)), whether Mo is co-implanted or not. The release of Cs is also similar (62±5 % without Mo, 57±5 % with Mo). Therefore, we conclude that the co-implantation of Mo and Cs does not change the overall behaviour of Cs, but induces a strong mobility of Mo.

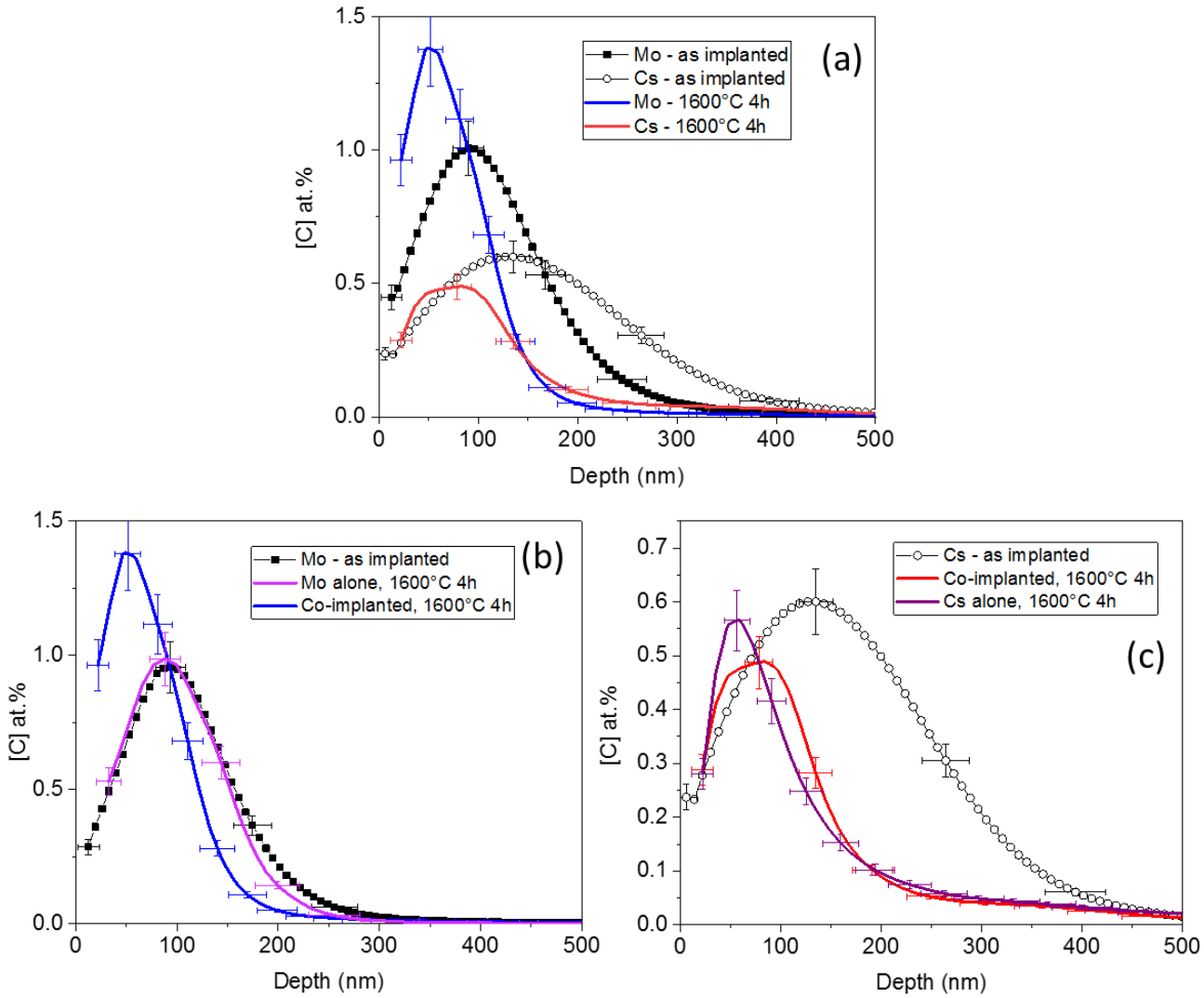

Figure 2: Molybdenum and caesium concentration profiles in UO_2 before and after annealing 4 hours at 1600°C under 5% H_2/Ar atmosphere. Shown are the results from a co-implanted sample (a) and a UO_2 sample containing either Mo (b) or Cs (c) only. Error bars were determined from SIMS resolution.

3.2. Microstructural characterization by TEM.

We have seen that, when either Mo or Cs are the only element present in UO_2, they exhibit a very different behaviour after thermal treatments under reducing conditions. We were able to explain it by microstructural and spectroscopic studies. Indeed, we have shown in a previous study that, after annealing, the major part of remaining Cs is found accumulated at a 50 nm depth from the surface in the form of bubbles [18]. In the case of Mo, we have observed it to be in a metallic form [23]. Further TEM analysis on an annealed UO_2 sample implanted with molybdenum at high concentration confirms these results, by showing the formation of metallic precipitates. This behaviour, visible in Figure 3 where the darker round shaped areas correspond to the Mo precipitates. Indeed, diffraction measurements were carried out and the measured lattice parameter was found equal to 0.33 nm,

which corresponds to metallic Face-centred cubic Mo. The formation of these precipitates could explain the observed immobility of Mo in absence of Cs.

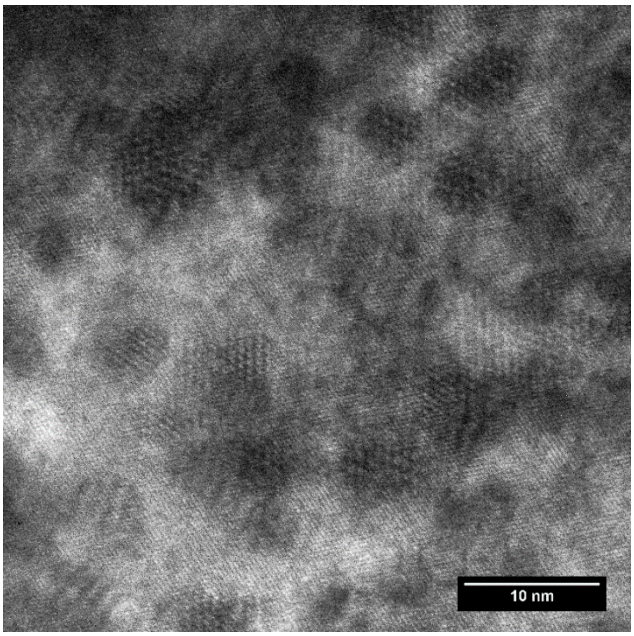

Figure 3: TEM image of a UO_2 sample implanted with Mo (5 10^{16} at/cm²) and annealed at 1600°C under 5% H_2/Ar atmosphere for 4 hours.

In order to get insights into the behaviour of Mo and Cs when they are co-implanted in UO_2 samples, TEM analyses were carried out.

3.2.1. UO_2 samples after co-implantation of Mo and Cs

Figure a) and 4b) shows the micrograph of a UO_2 pellet after implantation of Mo and Cs over the first 300 nm. The concentration profiles of these elements, obtained by SIMS, are superimposed to the TEM image on figure 4a as well as the dpa profiles calculated by SRIM. As already pointed out for a UO_2 sample implanted only with Cs at a 10^{15} at/cm² fluence [18], three zones can be identified as a function of the observed defects on these 2 micrographs. In the first 100 nm below the surface, few extended defects are visible whereas a large number of point defects can be seen. This result agrees well with the fact that this zone roughly corresponds to the range within which most dpa are created by the ion implantation. Between 100 and 300 nm (zone 2), where most of Cs and Mo atoms are implanted, many extended defects are visible. They are created by the collision cascades occurring when ions stop in matter. The zone beyond 300 nm corresponds to the sample bulk free of defects. Figure 4c) is a higher magnification image of the first 150 nm of this sample, where some dislocation lines about 40 nm long are clearly visible. Their density was obtained using the 'line-intercept method' [26] which counts the number of intersections between dislocation lines and the five random lines in a TEM image, and we obtained a density of 5±2 x10^{15} m^{-2}. The uncertainty is estimated considering our experimental conditions. In this image, we also notice the presence of bright spherical features within the first 50 nm from the surface. They are better visualised by acquiring images in both underfocused (Figure a) and overfocused beam conditions (Figure 5b). In this way, cavities are observed that appear

as white spots when the image is underfocused and as black spots in the opposite case. These micrographs confirm the presence of small bubbles with a nanometer size, whose density was estimated at 6.8 10^{23} bubbles/m^3. Given the chemical nature of the elements implanted in the sample, we suppose that these cavities are bubbles filled with Cs atoms.

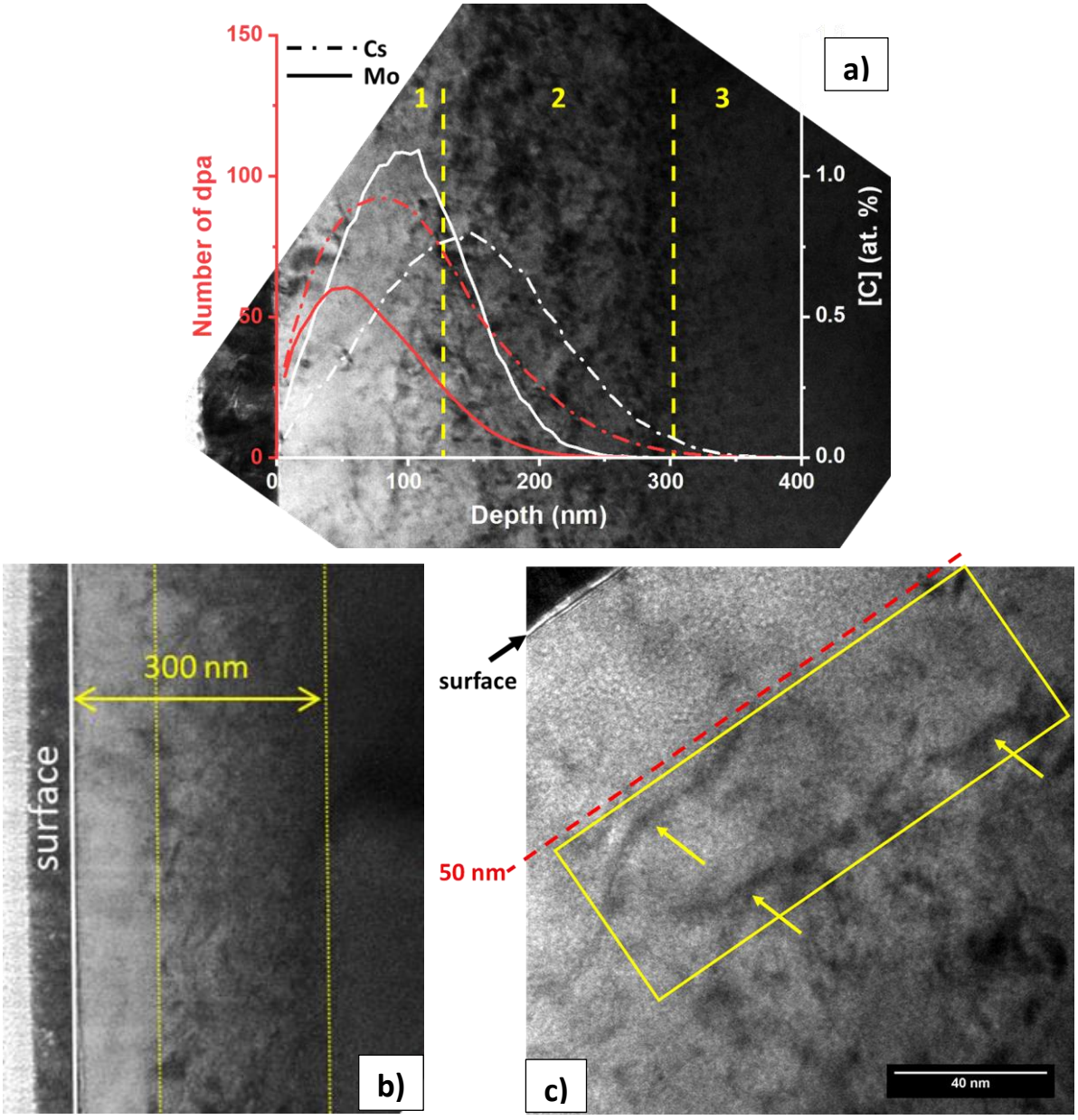

Figure 4: TEM images of a UO_2 sample co-implanted with molybdenum and caesium at 10^{16} at/cm². a) Cs and Mo concentration profiles obtained by SIMS have been superimposed as well as dpa profiles calculated by SRIM. b) visualisation of the 3 zones with different defects densities ; c) Same sample with a higher magnification, at which bubbles and dislocation lines (arrows) are visible.

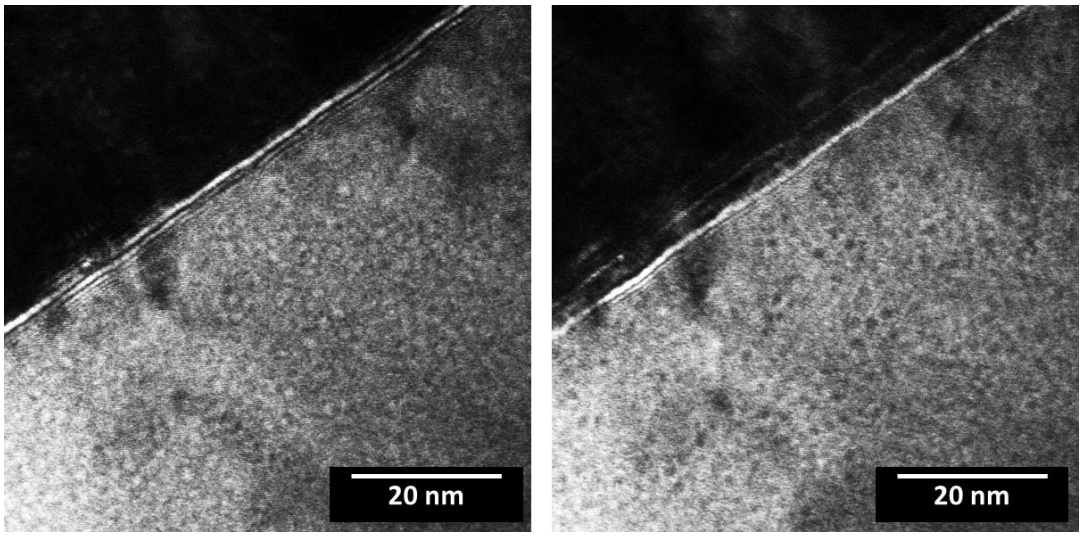

Figure 5: TEM images of an UO_2 sample co-implanted with molybdenum and caesium at 10^{16} at/cm² in underfocused (a) and overfocused beam conditions (b).

3.2.2. Cs and Mo co-implanted UO_2 after thermal annealing at 1600°C

Figure 6 shows a TEM image of a co-implanted sample after its annealing at 1600°C for 4 hours. One can observe that annealing caused a structuration of the Cs bubbles, which are now found distributed in two populations. The first one is located within the first 150 nm of the sample while some large faceted bubbles are visible along a line of dislocations located at a depth of about 350 nm (indicated by red arrows). Between these two agglomerations of bubbles, no extended defects are observed after the thermal treatment.

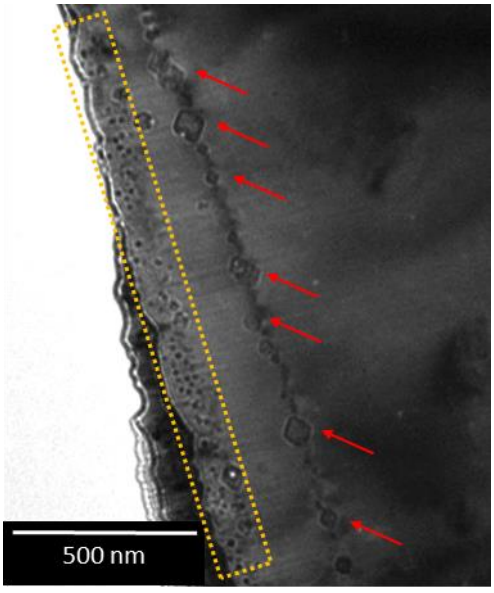

Figure 6: TEM image of a UO_2 sample co-implanted with Mo and Cs and annealed at 1600°C for 4 hours under reducing atmosphere.

An image of this sample at higher magnification is presented in Figure 7a). The Mo and Cs concentration profiles measured in this sample are superimposed, evidencing that the bubble

distribution within the first 150 nm matches well with the caesium concentration profile. Cs bubbles are present as either small spherical bubbles or facetted bubbles with a size ranging from 3 to 10 nm and with a total density estimated at 3.8 $10^{22}/m^3$. Some dark features are also visible in this area; blue arrows on figure 7a) point some of them out. High-resolution imaging in this region (shown in Figure b) evidences that these features correspond to metallic precipitates (recognizable from the Moiré fringes), composed of molybdenum and associated with caesium bubbles. The Mo precipitates have a size ranging from a few to 30 nm and they are anchored on dislocations, as can be seen on figure 7. Finally, some metallic precipitates are also associated to big faceted Cs bubbles (~ 30 nm in size) aligned along a dislocation horizontal region at about 350 nm from the surface. When we look at the Cs and Mo concentration profiles at this depth (see Figure 8), we can see that this bubble-precipitate alignment is correlated with a slight accumulation of both elements.

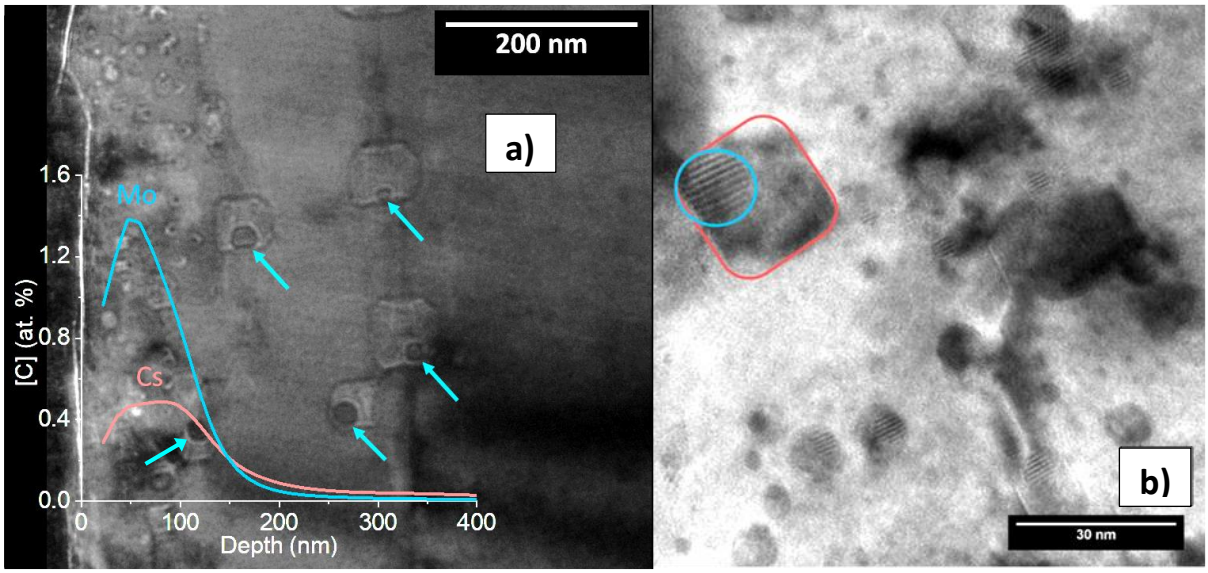

Figure 7: (a) TEM image of a UO_2 sample co-implanted with Mo and Cs and annealed at 1600°C for 4 hours. Cs and Mo SIMS profiles have been superimposed; (b) higher magnification image, highlighting a faceted bubble-metallic precipitate. Some pairs of bubble-metallic precipitates are visible in (a) and indicated by blue arrows.

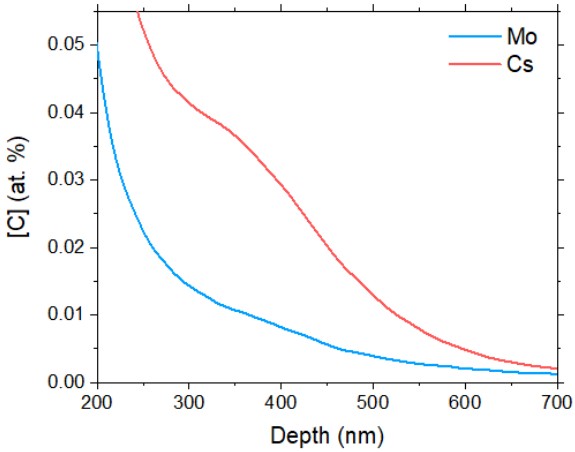

Figure 8: Concentration profiles of Cs and Mo in a UO_2 sample annealed at 1600°C for 4 hours, in the 200-700 nm depth range.

4. Discussion

The goal of our work was to characterize the influence of molybdenum on the behaviour of caesium in UO_2 at high temperature under reducing atmosphere. To this aim, we have implanted these two elements (Mo first, then Cs) in UO_2 pellets at a fluence of 10^{16} at/cm² each, which results in a maximum Mo concentration of 1 at % at 95 nm and Cs concentration of 0.6 at % at 140 nm. The implantation conditions were chosen so that the Mo and Cs concentration profiles overlap. After implantation, we have evidenced on the first 50 nm of the sample the presence of nanometric spherical cavities. Considering the chemical nature of Mo (metallic) and Cs (gaseous) under reducing conditions, we suppose that they correspond to Cs bubbles. The presence of ~~bubbles~~ such features at a higher depth cannot be ruled out even if they were not observed. This result is rather surprising, since bubbles have never been evidenced after Cs implantation in UO_2 samples, for previous experiments made for maximum Cs concentration ranging from 0.1 at.% [18, 27] to 2 at.% [17]. Actually, such Cs bubbles were only observed in UO_2 after annealing at low temperature (600°C for Sabathier et al [17], 1000°C for Panetier at al. [18]). However, Cs bubble formation at room temperature may be explained by the presence of Mo and the co-implantation sequence. Indeed, we have first implanted molybdenum atoms, creating numerous defects (vacancies, extended defects) in the first 200 nm of the UO_2 pellet. In particular, a large quantity of vacancies are created by the Mo implantation in the region where Cs bubbles were observed, as indicated by the dpa profile calculated by SRIM (cf Figure 1). We can thus formulate the hypothesis that the presence of these pre-existing defects makes possible the nucleation of bubbles during the Cs implantation. This process is possible according to theoretical calculations performed by Martin et al. [28]. These authors used molecular dynamics to simulate the effect of displacement cascades in UO_2. They show that a large part of vacancies created during the ions collision cascades are able to cluster together to form nano-cavities, which could constitute traps for atoms, such as Cs, which are poorly soluble in UO_2.

After the co-implantation, we have carried out thermal annealing at 1600°C under a reducing atmosphere and measured the evolution of the concentration profiles of Mo and Cs by SIMS. We evidenced that after 4 hours annealing both elements have migrated towards the surface, mainly

within the first 150 nm of the pellet. We have also measured a strong release of Cs during this annealing, whereas Mo accumulated towards the surface with a maximum concentration of 1.4 at.% at a mean depth of 50 nm. The behaviour of each element has to be compared with what happens when each of them is the only species present in UO_2 at the same concentration.

We have evidenced that Cs is very mobile in UO_2 when present alone, a large part being released from UO_2 while the rest either diffuses or is found in the form of bubbles towards the sample surface [18]. It is interesting to note that the Cs release is of the same order of magnitude whether there is molybdenum or not in the sample (~ 60 %) and that its final concentration profiles after annealing (with or without Mo) are rather similar (cf. Figure 2c), the remaining Cs being found towards the sample surface. We therefore conclude that the co-implantation does not change the overall migration behaviour of Cs in UO_2. As shown in Figure 2b), molybdenum is not mobile under the same annealing conditions at 1600°C when implanted alone in UO_2. It is known that the mobility of Mo is connected to the presence of defects in UO_2. Theoretical calculations showed that Mo atoms are better incorporated in uranium vacancies or Schottky defects, and that Mo migration occurs via a vacancy mechanism [29, 30]. Therefore, increasing the quantity of dpa (and thus uranium vacancies) created in UO_2 by ion implantation may enhance the Mo migration. This connexion between Mo migration and defects density in UO_2 is supported by the results obtained in one of our previous studies, in which we observed a Mo diffusion in UO_2 at 1600°C when this element was implanted at a high fluence of $5\ 10^{16}$ at/cm² (~4 at.% max) [23]. In the present study, defects due to Cs implantation are mainly created in the area where Mo atoms are present. We can therefore explain the mobility of Mo in presence of Cs by the increase of U vacancies created by the Cs implantation. However, the main Mo migration mechanism observed in presence of Cs is not diffusion, as in the case of [23], but a transport mechanism towards the surface. One may suppose that this movement is driven by the large amount of vacancies present towards the surface. As a result, Mo and Cs atoms remaining in the sample after annealing are distributed over the same depth.

We also evidence that the final elemental concentration distribution is correlated to Cs and Mo interactions, with the formation of Cs bubble-Mo precipitate pairs. The chemical behaviour of both elements is not influenced by the co-implantation: whether they are co-implanted or not in UO_2, Mo is found under the form of metallic precipitates, while the remaining caesium atoms formed bubbles after a 1600°C annealing. This chemical speciation of Mo under reducing conditions is in line with experimental observations of metallic precipitates in spent nuclear fuel [8, 31]. Evidence of metallic precipitate-gas bubble pairs in irradiated fuel has been found after high burn-up or high temperature treatments [1, 12-15]. All these authors suggest that the bubble-precipitate association would decrease the bubble coalescence rate and restrain the migration of bubbles in UO_2. It is clear from our work that the bubble migration is hindered by the formation of metallic precipitates. Indeed, we have shown previously that, in the absence of Mo, Cs is accumulated at a 50 nm depth [18]; conversely, in the present work, after the same thermal treatment (1600°C 4h) we observe Cs bubbles (3-10 nm) distributed over the same depth as molybdenum, i.e. within the first 150 nm. Thus, it seems that Mo metallic precipitates have anchored Cs bubbles. However, it is not possible to conclude firmly on the effect of Mo on the Cs bubble growth from our studies. Indeed, the same bubble features were characterized in presence or absence of Mo (spherical and faceted bubbles with a diameter ranging from 3 to 10 nm), but the initial Cs concentration is ten times higher in the present work.

We also observed in the TEM images the presence of some big bubble-precipitate pairs associated with dislocation lines aligned at about 350 nm from the surface. It corresponds to a slight accumulation of Cs and Mo, visible as small bumps on the SIMS profiles (cf. Figure 8). In this case, Cs bubbles are bigger than those present towards the surface (about 30 nm in diameter) and all faceted. Such post-annealing dislocation layer at the end of the Cs implantation zone was not observed in our previous study, in which Cs alone was implanted at the same fluence [18]. Its formation is probably the result of an accumulation of dislocations, which migrated during annealing. The evolution of the defect pattern in UO_2 has been studied by several authors [32-34] and with implantation parameters comparable to ours, in terms of energy loss and fluencies. The description of the defects observed in these works are in line with our works. The evolution from dislocation loops to lines has been found to also depend on the irradiation temperature, which were low (typically 600 °C) compared to the annealing temperatures used in our work. In a study of Staicu *et al.* [35] on the annealing of alpha defects having the same nature as those observed in this work it was shown that the defects in (U, Pu)O_2 become mobile at 400 °C for oxygen and 800 °C for uranium, respectively, whereas extended defects (loops) were annealed at higher temperature, i.e. 1000 °C. Also, the presence of Mo precipitates associated with Cs bubbles on this dislocation layer is in line with previous work on highly irradiated UO_2 at high temperature (1310°C), which evidenced that dislocations were anchored by metallic precipitates, and that gas bubbles were formed along dislocation lines [36]. Moreover, calculations showed that the presence of dislocations leads to a significant decrease in the U^{4+} diffusion activation energy in the region immediately surrounding the centre of the dislocation as compared to the bulk UO_2 lattice [37]. This increase in the U mobility, by pipe diffusion, will favor the segregation of bubbles in dislocations. It was also suggested that the formation of the high burn-up structure (HBS) could be explained by a dislocation reorganisation into sub-grains caused by dislocations piling up on the fission product precipitates [38]. It is interesting to note that in this region, we observe only big facetted bubbles, probably the result of an Ostwald ripening mechanism. The latter is favoured in this region, due to the low Cs concentration and the large amount of dislocations available. We can also notice in the micrograph in Figure 7 that a faceted bubble-precipitate pair is also present at ~170 nm, which roughly corresponds to the end of the Mo implantation range.

5. Conclusion

This study aims to evaluate the influence of a metallic fission product, molybdenum, on the behaviour of caesium in UO_2 at high temperature (1600°C). Both elements were introduced in the UO_2 matrix by ion implantation, and we have shown that the defects created by the Mo pre-implantation render possible the formation of nanometric cavities during the Cs implantation at room temperature. We suppose that they correspond to the nucleation of nanometric Cs bubbles. SIMS and TEM techniques were employed and their results coupled in order to characterize the migration of both elements, as well as the UO_2 microstructure evolution after annealing. We found that Mo is more mobile in presence of Cs, which may be related to an increase of available vacancies in the material produced by Cs implantation. On the contrary, the global behaviour of Cs remains quite similar: the released fraction of Cs during annealing was measured as ~60 % both in absence and in presence of Mo, and the remaining Cs is found in the form of bubbles with a size ranging from 3 to 10 nm. However, both elements are found distributed over the same depth (~150 nm) after annealing, as Mo metallic precipitates and Cs bubbles, which have been shown to be associated to each other. This is in line with

observations made in burn-up fuel, which confirms that our experimental methodology using ion implantation to introduce fission products is representative of reactor conditions.

These experiments were made under reducing conditions that do not favour chemical interactions between Cs and Mo and they highlight the role of dislocations on the nucleation of bubbles and metallic precipitates. As a next step, it will be interesting to see the evolution of these bubble/precipitate pairs under oxidizing conditions that may likely occur during an accidental sequence.

Acknowledgments

The authors acknowledge A. Duranti (IP2I Lyon, France) for the ion implantation on IMIO400 accelerator and Dr. Philippe Sainsot for interferometry measurements (INSA Lyon, France). Acknowledgements go to the InnoEnergy PhD School Programme and the European Institute of Technology (EIT) for the financial support and to JRC Karlsruhe for the internship position.

References

[1] L.E. Thomas, C.E. Beyer, L.A. Charlot, Microstructural analysis of LWR spent fuels at high burnup, J. Nucl. Mater., 188 (1992) 80. https://doi.org/10.1016/0022-3115(92)90457-V.
[2] J.-P. Hiernaut, T. Wiss, J.Y. Colle, Fission product release and microstructure changes during laboratory annealing of a very high burn-up fuel specimen, J. Nucl. Mater., 377 (2008) 313. doi:10.1016/j.jnucmat.2008.03.006.
[3] C.T. Walker, S. Bremier, S. Portier, R. Hasnaoui, W. Goll, SIMS analysis of an UO_2 fuel irradiated at low temperature to 65 MWd/kgHM, J. Nucl. Mater., 393 (2009) 212. doi:10.1016/j.jnucmat.2009.06.017.
[4] G. Ducros, P.P. Malgouyres, M. Kissane, D. Boulaud, M. Durin, Fission product release under severe accidental conditions: General presentation of the program and synthesis of VERCORS 1-6 results, Nucl. Eng. Des., 208 (2001) 191. DOI: 10.1016/S0029-5493(01)00376-4.
[5] Y. Pontillon, E. Geiger, C.L. Gall, S. Bernard, A. Gallais-During, P.P. Malgouyres, E. Hanus, G. Ducros, Fission products and nuclear fuel behaviour under severe accident conditions part 1: Main lessons learnt from the first VERDON test, J. Nucl. Mater., 495 (2017) 363. http://dx.doi.org/10.1016/j.jnucmat.2017.08.021.
[6] T. Kudo, M. Kida, T. Nakamura, F. Nagase, T. Fuketa, Releases of cesium and poorly volatile elements from UO_2 and MOx fuels under severe accident conditions, J. Nucl. Sci. Technol., 44 (2007) 1421. https://doi.org/10.1080/18811248.2007.9711389.
[7] E. Geiger, Study of fission products (Ba, Cs, Mo, Ru) behaviour in irradiated and simulated nuclear fuels during severe accidents using X-ray absorption spectroscopy, SIMS and EPMA, Thesis, University Paris-Saclay, France, (2016).
[8] H. Kleykamp, The chemical state of the fission products in oxide fuels, J. Nucl. Mater., 131 (1985) 221. https://doi.org/10.1016/0022-3115(85)90460-X.
[9] T. Adachi, T. Muromura, H. Takeishi, T. Yamamoto, Metallic phases precipitated in UO_2 fuel. II. Insoluble residue in simulated fuel., J. Nucl. Mater., 160 (1988) 81. https://doi.org/10.1016/0022-3115(88)90011-6.
[10] T. Muromura, T. Adachi, H. Takeishi, Z. Yoshida, T. Yamamoto, K. Ueno, Metallic phases precipitated in UO_2 fuel. I. Phases in simulated fuel., J. Nucl. Mater., 151 (1988) 327. https://doi.org/10.1016/0022-3115(88)90027-X.

[11] I. Sato, H. Furuya, K. Idemitsu, T. Arima, K. Yamamoto, M. Kajitani, Distribution of molybdenum in FBR fuel irradiated to high burnup, J. Nucl. Mater., 247 (1997) 46. https://doi.org/10.1016/S0022-3115(97)00062-7.
[12] A.D. Whapham, Electron Microscope Observation of the Fission-Gas Bubble Distribution in UO_2, Nucl. Appl., 2:2 (1966) 123. https://doi.org/10.13182/NT66-A27492.
[13] A.J. Manley, Transmission electron microscopy of irradiated UO_2 fuel pellets, J. Nucl. Mater., 27 (1968) 216. https://doi.org/10.1016/0022-3115(68)90125-6.
[14] I.J. Hastings, Bubble-precipitate interaction on grain boundaries in irradiated UO_2, J. Nucl. Mater., 54 (1974) 138. https://doi.org/10.1016/0022-3115(74)90084-1.
[15] C.T. Walker, P. Knappik, M. Mogensen, Concerning the development of grain face bubbles and fission gas release in UO_2 fuel, J. Nucl. Mater., 160 (1988) 10. https://doi.org/10.1016/0022-3115(88)90003-7.
[16] I.L.F. Ray, H. Thiele, H. Matzke, Transmission electron microscopy study of fission product behaviour in high burnup UO_2, J. Nucl. Mater., 188 (1992) 90. https://doi.org/10.1016/0022-3115(92)90458-W.
[17] C. Sabathier, L. Vincent, P. Garcia, F. Garrido, G. Carlot, L. Thomé, P. Martin, C. Valot, In situ TEM study of temperature-induced fission product precipitation in UO_2, Nucl. Instr. and Meth. in Phys. Res. B, 266 (2008) 3027. doi:10.1016/j.nimb.2008.03.158.
[18] C. Panetier, Y. Pipon, C. Gaillard, N. Moncoffre, T. Wiss, D. Mangin, O. Dieste, R. Ducher, R. Dubourg, B. Marchand, T. Epicier, L. Raimbault, Caesium thermal migration in UO_2: a comparative study with the xenon behavior, J. Nucl. Mater., (In press). DOI:10.1016/j.jnucmat.2020.152520.
[19] N. Djourelov, B. Marchand, H. Marinov, N. Moncoffre, Y. Pipon, P. Nedelec, N. Toulhoat, Variable energy positron beam study of Xe-implanted uranium oxide, J. Nucl. Mater., 432 (2013) 287. http://dx.doi.org/10.1016/j.jnucmat.2012.07.035.
[20] J.F. Ziegler, M.D. Ziegler, J.P. Biersack, SRIM - The stopping and range of ions in matter, Nucl. Instr. and Meth. in Phys. Res. B, 268 (2010) 1818. https://doi.org/10.1016/j.nimb.2010.02.091.
[21] J. Soullard, High voltage microscope observations of UO_2, J. Nucl. Mater., 135 (1985) 190. https://doi.org/10.1016/0022-3115(85)90077-7.
[22] P. Peres, S.-Y. Choi, F. Desse, P. Bienvenu, I. Roure, Y. Pipon, C. Gaillard, N. Moncoffre, L. Sarrasin, D. Mangin, Dynamic SIMS for materials analysis in nuclear science, J. Vac. Sci. Technol. B, 36 (2018) 03F117. https://doi.org/10.1116/1.5017027.
[23] L. Sarrasin, C. Gaillard, C. Panetier, Y. Pipon, N. Moncoffre, D. Mangin, R. Ducher, M. Dubourg, Effect of the Oxygen Potential on the Mo Migration and Speciation in UO_2 and UO_{2+x}, Inorg. Chem., 58 (2019) 4761. DOI: 10.1021/acs.inorgchem.8b03076.
[24] L. Sarrasin, Y. Pipon, C. Gaillard, N. Moncoffre, N. Bérerd, P. Simon, D. Mangin, R. Ducher, M. Dubourg, Influence of temperature and electronic stopping power of UO_2 irradiated with swift ions on Mo migration, Nucl. Instr. and Meth. in Phys. Res. B, 435 (2018) 111. https://doi.org/10.1016/j.nimb.2017.12.020.
[25] T. Wiss, H. Thiele, A. Janssen, D. Papaioannou, V. Rondinella, R.J.M. Konings, Recent Results of Microstructural Characterization of Irradiated Light Water Reactor Fuels using Scanning and Transmission Electron Microscopy, JOM, 64 (2013) 1390. https://doi.org/10.1007/s11837-012-0483-1.
[26] U. Martin, U. Mühle, H. Oettel, Erfahrungen mit der quantitativen Bestimmung der Versetzungsdichte im Transmissionselektronenmikroskop, Praktische Metallographie, 32 (1995) 467.
[27] C. Panetier, Etude des mécanismes de migration du césium dans le dioxyde d'uranium stoechiométrique et sur-stoechiométrique : influence du molybdène, University of Lyon, (2019).
[28] G. Martin, P. Garcia, C. Sabathier, L.V. Brutzel, B. Dorado, F. Garrido, S. Maillard, Irradiation-induced heterogeneous nucleation in uranium dioxide, Phys. Lett. A, 374 (2010) 3038. doi:10.1016/j.physleta.2010.05.033.
[29] G. Brillant, F. Gupta, A. Pasturel, Investigation of molybdenum and caesium behaviour in urania by ab initio calculations, J. Phys.: Condens. Matter., 21 (2009) 285602. https://doi.org/10.1088/0953-8984/21/28/285602.

[30] S. Nicoll, H. Matzke, R.W. Grimes, C.R.A. Catlow, Behaviour of single atoms of molybdenum in urania, J. Nucl. Mater., 240 (1997) 185. https://doi.org/10.1016/S0022-3115(96)00716-7.
[31] H. Kleykamp, The solubility of selected fission products in UO_2 and $(U,Pu)O_2$, J. Nucl. Mater., 206 (1993) 82. https://doi.org/10.1016/0022-3115(93)90236-R.
[32] C. Onofri, C. Sabathier, H. Palancher, G. Carlot, S. Miro, Y. Serruys, M. Legros, Evolution of extended defects in polycristalline UO_2 under heavy ion irradiation: Combined TEM, XRD and Raman study, Nucl. Instr. and Meth. in Phys. Res. B, 374 (2016) 51. http://dx.doi.org/10.1016/j.nimb.2015.08.091.
[33] C. Onofri, C. Sabathier, C. Baumier, C. Bachelet, H. Palancher, B. Warot-Fonrose, M. Legros, Influence of exogenous xenon atoms on the evolution kinetics of extended defects in polycrystalline UO_2 using in situ TEM, J. Nucl. Mater., 512 (2018) 297. https://doi.org/10.1016/j.jnucmat.2018.10.025.
[34] L.-F. He, M. Gupta, C.A. Yablinsky, J. Gan, M.A. Kirk, X.-M. Bai, J. Pakarinen, T.R. Allen, In situ TEM observation of dislocation evolution in Kr-irradiated UO_2 single crystal, J. Nucl. Mater., 443 (2013) 71. http://dx.doi.org/10.1016/j.jnucmat.2013.06.050.
[35] D. Staicu, T. Wiss, V.V. Rondinella, J.-P. Hiernaut, R.J.M. Konings, C. Ronchi, Impact of auto-irradiation on the thermophysical properties of oxide nuclear reactor fuels, J. Nucl. Mater., 397 (2010) 8. doi:10.1016/j.jnucmat.2009.11.024.
[36] T. Sonoda, M. Kinoshita, I.L.F. Ray, T. Wiss, H. Thiele, D. Pellottiero, V.V. Rondinella, H. Matzke, Transmission electron microscopy observation on irradiation-induced microstructural evolution in high burn-up UO_2 disk fuel, Nucl. Instr. and Meth. in Phys. Res. B, 191 (2002) 622. https://doi.org/10.1016/S0168-583X(02)00622-5.
[37] S.T. Murphy, E.E. Jay, R.W. Grimes, Pipe diffusion at dislocations in UO_2, J. Nucl. Mater., 447 (2014) 143. http://dx.doi.org/10.1016/j.jnucmat.2013.12.029.
[38] V. Rondinella, T. Wiss, The high burn-up structure in nuclear fuel, Mater. Today, 13 (2010) 24. https://doi.org/10.1016/S1369-7021(10)70221-2.